

1 ***Suzaku* X-ray Imaging of the Extended Lobe in the Giant Radio Galaxy**
 2 **NGC 6251 Associated with the *Fermi*-LAT Source 2FGL J1629.4+8236**

3 Y. Takeuchi¹, J. Kataoka¹, Ł. Stawarz^{2,3}, Y. Takahashi¹, K. Maeda¹, T. Nakamori¹,
 4 C. C. Cheung⁴, A. Celotti⁵, Y. Tanaka², and T. Takahashi²

5 uto_of_take@suou.waseda.jp

6 **ABSTRACT**

7 We report the results of a *Suzaku* X-ray imaging study of NGC 6251, a nearby giant radio galaxy with intermediate FR I/II radio properties. Our pointing direction was centered on the γ -ray emission peak recently discovered with *Fermi*-LAT around the position of the north-west radio lobe 15 arcmin offset from the nucleus. After subtracting two “off-source” pointings adjacent to the radio lobe, and removing possible contaminants in the XIS field of view, we found significant residual X-ray emission most likely diffuse in nature. The spectrum of the excess X-ray emission is well fit by a power law with photon index $\Gamma = 1.90 \pm 0.15$ and a 0.5 – 8 keV flux of 4×10^{-13} erg cm⁻² s⁻¹. We interpret this diffuse X-ray emission component as being due to inverse-Compton up-scattering of the cosmic microwave background photons by ultrarelativistic electrons within the lobe, with only a minor contribution from the beamed emission of the large-scale jet. Utilizing archival radio data for the source, we demonstrate by means of broad-band spectral modeling that the γ -ray flux of the *Fermi*-LAT source 2FGL J1629.4+8236 may well be accounted for by the high-energy tail of the inverse-Compton continuum of the lobe. Thus, this claimed association of γ -rays from the north-west lobe of NGC 6251, together with the recent *Fermi*-LAT imaging of the extended lobes of Centaurus A, indicates that particles may be efficiently (re-)accelerated up to ultrarelativistic energies within extended radio lobes of nearby radio galaxies in general.

¹Research Institute for Science and Engineering, Waseda University, 3-4-1 Okubo, Shinjuku, Tokyo, 169-8555, Japan.

²Institute of Space and Astronautical Science (ISAS), Japan Aerospace Exploration Agency (JAXA), 3-1-1 Yoshinodai, Chuo-ku, Sagami-hara, Kanagawa, 252-5510 Japan

³Astronomical Observatory, Jagiellonian University, ul. Orla 171, Kraków 30-244, Poland

⁴National Research Council Research Associate, National Academy of Sciences, Washington, DC 20001, resident at Naval Research Laboratory, Washington, DC 20375, USA

⁵Scuola Internazionale Superiore di Studi Avanzati (SISSA), 34014 Trieste, Italy

8 *Subject headings:* acceleration of particles — radiation mechanisms: non-thermal —
9 X-rays: galaxies — gamma rays: general — galaxies: jets — galaxies: individual
10 (NGC 6251)

11 **1. Introduction**

12 With the successful launch of the *Fermi* Gamma-ray Space Telescope, we now have an un-
13 precedented opportunity to study in detail the γ -ray emission from different types of astrophysical
14 sources. The 2FGL catalog (Abdo et al. 2011)¹ contains 1873 sources detected in the 100 MeV to
15 100 GeV range by the Large Area Telescope (LAT) onboard the *Fermi* satellite during the first 24
16 months of the science phase of the mission, which began on 2008 August 4. Among 1297 objects
17 included in 2FGL which are firmly identified or reliably associated with counterparts of known
18 source classes, more than half are blazars, i.e. active galactic nuclei (AGN) with radiative outputs
19 dominated by a beamed jet emission. Non-blazar AGN constitute only a small fraction ($\simeq 3\%$) of
20 the identified 2FGL population, but nonetheless have already emerged as a new, important, and at
21 the same time relatively diverse class of γ -ray emitters. The second catalog of AGN detected by
22 *Fermi*-LAT (2LAC; Ackermann et al. 2011a) contains ten radio galaxies, four narrow-line Seyfert
23 1 galaxies, and several other non-blazar-type AGN with prominent starburst components (see also
24 Abdo et al. 2010c; Ackermann et al. 2011b).

25 Particularly noteworthy in this context is the *Fermi*-LAT detection of the giant lobes in the
26 nearby radio galaxy Centaurus A, extending for about $\sim 5^\circ$ in the east-west direction, and $\sim 9^\circ$ in
27 the north-south direction ($\sim 300 \text{ kpc} \times 600 \text{ kpc}$ at the distance of 3.7 Mpc; Abdo et al. 2010b,d).
28 The *Fermi*-LAT results regarding the Centaurus A lobes have profound implications for the general
29 understanding of the evolution of radio galaxies, their interactions with the surrounding environ-
30 ment, and the production of high-energy particles in the Universe. In particular, prompted by these
31 recent results from the *Fermi*-LAT and also from the Pierre Auger Observatory (Abraham et al.
32 2007; Moskalenko et al. 2009), several authors have debated on the high-energy particle acceler-
33 ation and production of ultra high-energy cosmic rays within the giant lobes of Centaurus A and
34 similar systems (Hardcastle et al. 2009; O’Sullivan et al. 2009; Pe’er & Loeb 2011).

35 Besides Centaurus A, three other radio galaxies detected so far with *Fermi*-LAT could be
36 promising targets for investigating the extended γ -ray emission components associated with radio
37 lobes. Prior to the launch of *Fermi*, Cheung (2007) and Georganopoulos et al. (2008) pointed
38 out that the radio lobes of Fornax A might be detected at GeV energies and seen as extended

¹See also the online version at http://fermi.gsfc.nasa.gov/ssc/data/access/lat/2yr_catalog/

39 structures by the LAT but its associated 2FGL source is faint and currently appears to be a point-
 40 source (Abdo et al. 2011). Similarly, the γ -ray emission associated with Centaurus B and reported
 41 recently in 2LAC may be dominated by the lobes, but due to a relatively small angular size of
 42 the source ($\sim 0.^\circ 2$ in the north-south direction) careful analysis of the *Fermi*-LAT data is needed
 43 before drawing any robust conclusions (Katsuta et al. in prep). The giant radio galaxy NGC 6251
 44 already appeared in the first-year *Fermi*-LAT catalog (1FGL; Abdo et al. 2010a) and is another
 45 object worth attention due to the large angular extent of its radio structure ($\sim 1.^\circ 2$) which in
 46 principle could be resolved with *Fermi*-LAT above 1 GeV photon energies. Based on the one-year
 47 of accumulated LAT data, the NGC 6251 nucleus was included within the 95% LAT error ellipse
 48 of 1FGL J1635.4+8228, and its reported γ -ray flux could be due to the unresolved nuclear jet of the
 49 radio galaxy (Migliori et al. 2011). Subsequently however, the position of the 2FGL counterpart
 50 of NGC 6251, namely 2FGL J1629.4+8236 (detected at 12σ level), is now shifted north-west with
 51 respect to the 1FGL source position, toward the outer jet and radio lobe. We note that previously,
 52 the NGC 6251 galaxy was proposed to be associated with the EGRET source 3EG J1621+8203
 53 (Mukherjee et al. 2002).

54 NGC 6251 is a nearby AGN hosting a supermassive black hole with a mass, $M_{\text{BH}} \simeq (4 -$
 55 $8) \times 10^8 M_\odot$ (Ferrarese & Ford 1999; Ho 2002). It is classified as an FR I radio galaxy (Laing et al.
 56 1983) based on its jet morphology and monochromatic 178 MHz luminosity of $1.9 \times 10^{24} \text{ W Hz}^{-1} \text{ sr}^{-1}$
 57 (Waggett et al. 1977), although the entire giant radio structure resembles more FR II or interme-
 58 diate FR I/FR II systems (Schoenmakers et al. 2001). At the distance of $\sim 106 \text{ Mpc}$ ($z = 0.0247$,
 59 conversion scale 0.491 kpc/arcsec ; Wegner et al. 2003) the linear extension of the lobes reads as
 60 $\simeq 2.1 \text{ Mpc}$, which is a larger physical size than that covered by the outer lobes of Centaurus A.
 61 The radio jet in NGC 6251, discussed in detail in (Perley et al. 1984), is likely to be relativistic
 62 up to large distances from the core and observed at viewing angles $\theta_j \lesssim 40 \text{ deg}$, as suggested by
 63 the jet-to-counterjet brightness asymmetry on both pc and kpc scales. It can be divided into (i)
 64 the bright inner region within the first $\sim 120''$, (ii) a faint central part extending from $\sim 120''$
 65 up to $\sim 180''$, (iii) the *outer region* flaring between $\sim 180''$ and $\sim 270''$, and (iv) a curved and
 66 low-surface brightness tail beyond $\sim 270''$. The outer jet region has been detected at X-ray fre-
 67 quencies by *ROSAT* (Birkinshaw & Worrall 1993; Mack et al. 1997b), *XMM-Newton* and *Chandra*
 68 (Sambruna et al. 2004a; Evans et al. 2005). The origin of the detected jet X-ray emission is still
 69 an open question and different models have been discussed for such, including thermal emission
 70 (Mack et al. 1997b), beamed inverse-Compton radiation (Sambruna et al. 2004a), and synchrotron
 71 process (Sambruna et al. 2004a; Evans et al. 2005). However, none of the previous X-ray observa-
 72 tions pointed to either the north-west or south-east lobe regions, separated by $\sim 0.^\circ 3$ and $\sim 0.^\circ 7$
 73 from the NGC 6251 nucleus, respectively.

74 In this paper, we present the results of the newly conducted observations of NGC 6251 with the
 75 *Suzaku* X-ray satellite (Mitsuda et al. 2007) mainly in 2011 April. NGC 6251 was first observed by

76 *Suzaku* in 2010 December (Evans et al. 2011), but these observations targeted strictly the nucleus
 77 of the radio galaxy. This time the pointing direction was intentionally shifted 15 arcmin in the
 78 north-west direction from the nucleus in order to study the γ -ray emission peak discovered with
 79 *Fermi*-LAT around the position of the NW radio lobe. In § 2, we describe the *Suzaku* observations
 80 and data reduction procedure. The results of the analysis are given in § 3. The discussion and
 81 conclusions are presented in § 4 and § 5, respectively.

82 2. *Suzaku* Observations and Data Reduction

83 *Suzaku* is the ideal instrument for the intended study since it provides a low and stable Non
 84 X-ray Background (NXB), particularly for diffuse sources (Mitsuda et al. 2007; Tawa et al. 2008).
 85 We have therefore observed the NW lobe in NGC 6251 for 34.2 ksec (“on” pointing). In addition,
 86 two short observations (18.8 ksec and 12.1 ksec) were made in the vicinity of the radio lobe in
 87 order to estimate the background flux (“off” pointings). Hereafter, we denote these three obser-
 88 vations as LOBE, BGD1, and BGD2, respectively, and the observation log is provided in Table 1.
 89 Both BGD1 and BGD2 observations were made just after the LOBE observation so that the long-
 90 term background fluctuation as well as possible effects caused by the detector degradation can be
 91 minimized. In the case of BGD2, an additional short (11.1 ksec) exposure was obtained in 2011
 92 August, but these data were excluded from the analysis presented here to avoid possible artifacts
 93 related to the aforementioned problems. We have checked that the presented results do not change
 94 within statistical errors when the additional BGD2 data are included in the spectral analysis.

95 The observations were made with X-ray Imaging Spectrometer (XIS; Koyama et al. 2007)
 96 which consists of four CCD cameras each placed in the focal plane of the X-ray Telescope (XRT;
 97 Serlemitsos et al. 2007), and with the Hard X-ray Detector (HXD; Kokubun et al. 2007; Takahashi et al.
 98 2007). Each XIS covers a $18' \times 18'$ region on the sky, which is sufficiently large to include the
 99 whole NW lobe within a single pointing image. On the other hand, since HXD is a non-imaging
 100 instrument with a large field of view $34' \times 34'$ (Takahashi et al. 2007) and we cannot discriminate
 101 between the hard X-ray emission from the nucleus (Evans et al. 2011) and possible emission from
 102 the extended NW radio lobe in the HXD data, we only use the imaging and spectral results obtained
 103 with XIS in this paper. One of the XIS sensors (XIS 1) has a back-illuminated (BI) CCD, while the
 104 other three (XISs 0, 2, and 3) utilize front-illuminated (FI) CCDs. Because of an anomaly in 2006
 105 November, the operation of XIS2 has been terminated and we use only three CCDs. The XIS was
 106 operated in the normal full-frame clocking mode with the 3×3 or 5×5 editing mode.

107 In our *Suzaku* pointing, the relatively bright NGC 6251 nucleus was located well outside the
 108 field of view of the XIS. However, due to the relatively large point spread function of the XRT
 109 onboard *Suzaku* (half power diameter of $\simeq 2.0'$; Serlemitsos et al. 2007), the contamination of the

110 NGC 6251 nucleus may still, in principle, affect the exposure of the NW radio lobe: the pointing
 111 center of our LOBE observation is separated by only $\sim 15'$ from the core. For this reason, we
 112 simulated the contamination effect using `xissim`. In the simulation, we assumed a point source
 113 at the position of the nucleus characterized by a power-law continuum with the photon index, $\Gamma =$
 114 1.87, and the normalization $K = 6.79 \times 10^{-4}$ photons keV $^{-1}$ cm $^{-2}$ s $^{-1}$ at 1 keV (corresponding
 115 to the 2 – 10 keV unabsorbed luminosity 2.8×10^{42} erg s $^{-1}$), as reported in (Evans et al. 2011).
 116 We found that the expected net count rate (the XIS count rate for the “on” pointing subtracted by
 117 the background count rate estimated from the “off” pointings) for the region used in the spectral
 118 analysis (see § 3.2 below) due to the core contamination is 4.11×10^{-4} s $^{-1}$ only, whilst the total
 119 source net count rate is 6.40×10^{-2} s $^{-1}$. Hence, we conclude that the leakage effect is at the
 120 level of about 0.64 %, and so that the stray light contamination from the NGC 6251 nucleus can be
 121 considered as negligible when analyzing the diffuse emission of the NW lobe.

122 We analyzed the screened XIS data, reduced using the *Suzaku* software version 1.2. The
 123 screening was based on the following criteria: (1) only ASCA-grade 0, 2, 3, 4, 6 events were accu-
 124 mulated, while hot and flickering pixels were removed from the XIS image using the `sisclean`
 125 script (Day et al. 1998), (2) the time interval after the passage of South Atlantic Anomaly was
 126 greater than 60 s, (3) the object was at least 5° and 20° above the rim of the Earth (ELV) during
 127 night and day, respectively. In addition, we also selected the data with a cutoff rigidity (COR)
 128 larger than 6 GV. In the reduction and the analysis of the *Suzaku* XIS data, HEADAS software
 129 version 6.11 and a calibration databases (CALDB) released on 2009 September 25 were used.
 130 The XIS cleaned event data-set was obtained in the combined 3×3 and 5×5 edit modes using
 131 `xselect`. We note that no spectral variability were observed in the XIS data and the imaging and
 132 spectral analyses are discussed in the next section.

133 3. X-ray Analysis

134 3.1. Image Analysis

135 We extracted the XIS images within the photon energy range of 0.4 – 10 keV from only the
 136 two FI CCDs (XIS 0, XIS 3) because the BI CCD (XIS1) has lower imaging quality. In the image
 137 analysis, we excluded calibration sources at the corner of the CCD chips. The images of the NXB
 138 were obtained from the night Earth data using `xisnxbgen` (Tawa et al. 2008). Since the exposure
 139 times for the original data were different from that of NXB, we calculated the appropriate exposure-
 140 corrected original and NXB maps using `xisexpmapgen` (Ishisaki et al. 2007). The corrected
 141 NXB images were next subtracted from the corrected original images. In addition, we simulated
 142 flat sky images using `xissim` (Ishisaki et al. 2007), and applied a vignetting correction. All the

143 images obtained with XIS0 and XIS3 were combined and rebinned by a factor of 4 (CCD pixel
 144 size $24\ \mu\text{m} \times 24\ \mu\text{m}$, so that 1024×1024 pixels cover an $18' \times 18'$ region on the sky; Koyama et al.
 145 2007). Throughout these processes, we also performed vignetting correction for all the XIS images
 146 for LOBE, BGD1 and BGD2. Finally, the images were smoothed with a Gaussian function with
 147 $\sigma = 0.28''$.

148 The resulting XIS images are shown in Figure 1, with a 325 MHz radio contours of NGC 6251
 149 (Mack et al. 1997a) and the 95% LAT error circle of 2FGL J1629.4+8236 overlaid. When compar-
 150 ing the LOBE, BGD1, and BGD2 images, one can clearly see an excess X-ray emission possibly
 151 associated with the NW radio lobe. The apparent enhancements at the edges of the XIS images are
 152 artifacts due to an insufficient exposure at the CCD edges caused by small fluctuation of attitude
 153 during the observation. Interestingly, at the sensitivity limit of these *Suzaku* observations, no ex-
 154 cess X-ray emission was detected from the bright radio hotspot located at the edge of the lobe. In
 155 the context of the study by Hardcastle et al. (2004), since NGC 6251 is a low power FR I/II source,
 156 the X-ray emission from the hotspot is expected to be dominated by the high energy energy tail of
 157 the synchrotron continuum rather than by the inverse-Compton component. Specifically, the radio
 158 flux of the hotspot of 0.1 Jy at 1.5 GHz allows us to estimate roughly the expected X-ray flux by
 159 extrapolating the observed hotspot spectrum from lower frequencies as ~ 2 nJy. A point source
 160 at this flux level is easily detectable by *Chandra* or *XMM*, but our *Suzaku* non-detection is unsur-
 161 prising due to the relatively poor angular resolution of the instrument combined with a relatively
 162 intense diffuse emission of the surrounding lobe.

163 3.2. Spectral Analysis

164 In the spectral analysis, we extracted photons from the arc-like source region in the LOBE
 165 pointing as shown in Figure 2. This ‘arc-like region’ we are referring to is a part of a concentric ring
 166 centered at the radio core position of NGC 6251. There we excluded X-ray point sources detected
 167 by *ROSAT* (see the TABLE1 described in Mukherjee et al. 2002) as background contaminants,
 168 assuming the source region radii $2'$ (a typical half-power diameter of the XRT, as described above).
 169 We note that the origin of these X-ray features is still under debate, and hence it remains possible
 170 that they represent hotspot and enhancement related to the NW lobe itself. In our analysis, however,
 171 we removed all such bright X-ray spots, since the main objective of the paper is to detect and to
 172 characterize the *diffuse* X-ray emission component associated with the *diffuse* radio structure of
 173 the lobe. Similarly, we defined arc-like background regions for both BGD1 and BGD2 pointing
 174 using the same detector coordinates as chosen for the LOBE source region. We extracted the
 175 spectra from LOBE, BGD1 and BGD2 source regions with `xselect` for each CCD (XIS 0, XIS
 176 1, XIS 3). Spectral analysis and model fitting were performed with `xspec` version 12.7.0. In order

177 to improve the statistics, the spectra of XIS0 and XIS3 were summed together using `mathpha`.
 178 Moreover, the spectra of BGD1 and BGD2 were summed for the same reason in the same way.
 179 Finally, we made redistribution matrix files (RMFs) and ancillary response files (ARFs) using
 180 `xisrmfgen` and `xissimarfgen` (Ishisaki et al. 2007), respectively.

181 Using these RMFs and ARFs, the corrected spectrum about energy response and the effective
 182 area of XIS were obtained. Figure 3 shows the resulting (background subtracted) spectrum of
 183 the LOBE pointing within the energy range 0.4 – 7.5 keV. The spectrum could be well fitted by
 184 a single power-law continuum with a photon index, $\Gamma = 1.90 \pm 0.15$, moderated by the Galactic
 185 absorption only. The Galactic hydrogen column density was fixed as $N_{\text{H}} = 5.54 \times 10^{20} \text{ cm}^{-2}$
 186 (Dickey & Lockman 1990). The value of $\chi^2/\text{d.o.f} = 20.54/14$ indicates that this is a satisfac-
 187 tory model for the diffuse X-ray emission component of the NW lobe in NGC 6251. The details
 188 of the fitting results are summarized in Table 2. We note that, the spectrum is also equally well
 189 reproduced by a thin thermal plasma models (either bremsstrahlung and/or Raymond-Smith) mod-
 190 erated by Galactic absorption, with the temperature of $kT \gtrsim 3.7$ keV. This is rather high compared
 191 with those of thermal plasma of nearby elliptical galaxies (e.g, Matsushita, Ohashi, & Makishima
 192 2000). Moreover, the implied thermal pressure, $p_{\text{th}} \sim 2 \times 10^{-10} \text{ dyn cm}^{-2}$, is more than four orders
 193 of magnitude larger than the minimum-energy non-thermal pressure of the lobes (see, section 4.2).
 194 We regard these parameters as unrealistic, and hence we conclude that the diffuse X-ray emission
 195 component detected at the position of the NW lobe is purely non-thermal in origin.

196 4. Discussion

197 The analysis of *Suzaku* data for the NW lobe in NGC 6251 revealed the presence of X-ray
 198 emission, most likely of diffuse nature, well fitted by a power-law continuum with photon index
 199 $\Gamma \lesssim 2$ moderated by the Galactic absorption only. The 0.4 – 7.5 keV luminosity of the lobe corre-
 200 sponding to the *Suzaku* source extraction region reads as $5.4 \times 10^{41} \text{ erg s}^{-1}$. The detection of such a
 201 non-thermal X-ray emission component is interesting, but not exceptional, since several analogous
 202 detections of the X-ray lobes in either FR I or FR II radio galaxies have been previously reported
 203 (see Kataoka & Stawarz 2005; Croston et al. 2005; Isobe et al. 2011, and references therein). The
 204 relevance of our *Suzaku* observations of the NW lobe in NGC 6251 is due to the aforementioned
 205 possible (or even likely) association of the lobe with the *Fermi*-LAT source 2FGL J1629.4+8326.
 206 Note that in the case of the only radio galaxy for which the lobe emission was robustly associ-
 207 ated with a γ -ray source so far, Centaurus A, no diffuse X-ray emission component related to the
 208 extended radio structure has been detected (see in this context, Hardcastle et al. 2009). In other
 209 words, our observations may potentially provide the very first case of the detected X-ray emission
 210 from the large-scale lobe bright in γ -rays.

211 Yet the above statement may be considered as premature, since the 95% LAT error circle
 212 of 2FGL J1629.4+8236 includes not only the extended lobe but also the bright ‘outer jet’ re-
 213 gion (see § 1 and Figure 1). This region, as mentioned previously, has been resolved in X-rays
 214 before with *ROSAT*, *Chandra*, and *XMM-Newton* (Mack et al. 1997b; Sambruna et al. 2004a;
 215 Evans et al. 2005). Regardless of the debated origin of the jet-related X-ray photons (synchrotron
 216 versus beamed inverse-Compton), large scale jets detected at keV photon energies are in general
 217 thought to be the sites of efficient acceleration of high-energy electrons, and as such, to be potential
 218 sources of γ -rays detectable by modern instruments like *Fermi*-LAT (see, e.g., Stawarz et al. 2004;
 219 Sambruna et al. 2004b). Below we discuss in more detail the possible association of 2FGL J1629.4+8236
 220 with the outer jet and with the NW lobe of NGC 6251, and demonstrate by means of broad-band
 221 spectral modeling that the γ -ray flux can best be accounted for by the high-energy tail of the
 222 inverse-Compton continuum of the lobe.

223 4.1. Outer Jet

224 For the spectral modeling of the outer jet region, we take the 1.4 GHz flux density, $S_{1.4\text{GHz}} =$
 225 0.5 ± 0.05 Jy measured by Sambruna et al. (2004a) from a VLA map, and assume the radio spectral
 226 index $\alpha_r = 0.64 \pm 0.05$ within the 1 – 5 GHz range (Perley et al. 1984). We also approximate the
 227 X-ray spectrum of this region as a power-law with the photon index $\Gamma = 1.68 \pm 0.13$ within the
 228 0.4 – 7 keV range and the monochromatic flux $S_{1\text{keV}} = 4.7 \pm 0.4$ nJy, as given in Evans et al.
 229 (2005).² We approximate the jet as a cylinder with a radius $R_j = 5$ kpc and *projected* length
 230 $\ell_j = 40$ kpc so that the emitting volume is $V_j = \pi R_j^2 \ell_j / \sin \theta_j$.

231 We model the broad-band emission of the outer jet region in the framework of the beamed
 232 inverse-Compton scenario (Tavecchio et al. 2000; Celotti et al. 2001), with the radio emission be-
 233 ing due to the synchrotron radiation of non-thermal electrons distributed isotropically within a
 234 relativistic outflow, and the X-ray-to- γ -ray continuum due to Comptonization of the cosmic mi-
 235 crowave background (CMB) photons by the same electron population (‘beamed EC/CMB’ model
 236 below). Anisotropy of the CMB radiation in the jet rest frame, as well as Klein-Nishina effects,
 237 are properly taken into account (Stawarz et al. 2005). For simplicity, we assume homogeneous
 238 distributions of the radiating electrons and of the magnetic field within the whole outer jet region,
 239 which should be considered as a rough approximation only considering the observed asymmetric
 240 radio intensity and polarization transverse profiles of the outer jet (Perley et al. 1984).

²We note that slightly different X-ray spectral parameters for the outer jet region are claimed by Sambruna et al. (2004a), namely $S_{1\text{keV}} = 2.3 \pm 0.7$ nJy and $\Gamma = 1.15 \pm 0.38$ within the 0.5 – 9 keV range. Our re-analysis of archival *XMM-Newton* data is however more consistent with that of Evans et al. (2005).

241 As shown in Figure 4 (thin solid line), the γ -ray flux of 2FGL J1629.4+8236 is not well ac-
 242 counted for by the beamed EC/CMB model for the jet with the following ‘best fit’ parameters: the
 243 ratio between comoving electron and magnetic field energy densities $\eta_{\text{eq}} \equiv U'_e/U'_B = 1.75$, mag-
 244 netic field intensity $B = 2.3 \mu\text{G}$, jet bulk Lorentz factor $\Gamma_j = 3$, jet viewing angle $\theta_j = 17 \text{ deg}$, and
 245 the electron energy distribution of a power-law form $n'_e(\gamma) \propto \gamma^{-s} \times \exp[-\gamma/\gamma_{\text{max}}]$ with $s = 2.2$,
 246 $\gamma_{\text{min}} = 10$ and $\gamma_{\text{max}} = 5 \times 10^5$. With the above model parameters the observed ratio of the inverse-
 247 Compton and synchrotron peak luminosities reads as $L_{\text{ic}}/L_{\text{syn}} \simeq (\delta/\Gamma_j)^2 \times (U'_{\text{cmb}}/U'_B) \simeq 25$. Note
 248 however that the relatively small jet viewing angle implied by the model, $\theta_j = 17 \text{ deg}$, may be con-
 249 sidered as unlikely considering the large *projected* size of the whole radio structure of NGC 6251
 250 (see the related discussion in Evans et al. 2005). On the other hand, the implied jet kinetic lumi-
 251 nosities stored in electrons, magnetic field, and cold protons (assuming equal comoving number
 252 densities of protons and electrons), namely $L_e \simeq 0.7 \times 10^{44} \text{ erg s}^{-1}$, $L_B \simeq 0.4 \times 10^{44} \text{ erg s}^{-1}$, and
 253 $L_p \simeq 1.9 \times 10^{45} \text{ erg s}^{-1}$, giving the total jet power $L_j \simeq 2 \times 10^{45} \text{ erg s}^{-1}$, could be considered as
 254 reasonable values (Willott et al. 1999). This may imply that if the beamed EC/CMB model for the
 255 large-scale jet in NGC 6251 with the parameters as given above is realistic at all, the outer parts of
 256 the outflow may provide some contribution to the observed γ -ray flux of 2FGL J1629.4+8236, at
 257 least at the highest photon energies within the LAT range.

258 4.2. North-West Lobe

259 Next we consider the case of the NW lobe of NGC 6251 likely associated with the *Fermi*-
 260 LAT source 2FGL J1629.4+8236. For the purpose of the spectral modeling we measured radio
 261 fluxes for the lobe from published *WSRT* maps at 327 and 610 MHz (Mack et al. 1997a). Addi-
 262 tionally, we obtained a new VLA³ 1.56 GHz map at 45'' resolution with a total 5 hr integration
 263 from combining archival D-array observations obtained on 1985 December 1, 5, and 1986 Jan 18
 264 (programs AB346 and TEST). Our measurements, $S_{327 \text{ MHz}} = 3.10 \text{ Jy}$, $S_{610 \text{ MHz}} = 1.75 \text{ Jy}$, and
 265 $S_{1.56 \text{ GHz}} = 0.907 \text{ Jy}$, all assuming 10% errors, were measured using the same source extraction
 266 regions as in the *Suzaku* analysis (see Figure 2)⁴. The lobe also has a higher frequency radio flux
 267 measurement by Mack et al. (1997a), $S_{10.55 \text{ GHz}} = 213.5 \pm 26.4 \text{ mJy}$, and is detected and imaged
 268 down to 38 MHz (Rees 1990); due to the low resolution of the latter map, we summed the tabulated

³Calibrated data sets obtained from the NRAO VLA Archive Survey. The National Radio Astronomy Observatory is a facility of the National Science Foundation operated under cooperative agreement by Associated Universities, Inc.

⁴We note that the radio source extraction region includes a relatively bright radio hotspot mentioned already in section 3.1. By means of careful analysis of the available radio maps we have estimated the contribution of this hotspot to the total radio emission of the lobe as 10 % at most. i.e. at the level of the assumed radio flux measurement uncertainty

269 fluxes for the 3 components listed west of the central radio source to derive an upper limit to the
 270 lobe flux, $S_{38\text{MHz}} < 39.6\text{ Jy}$. Note that the emerging radio spectral index $\alpha_{0.326-10.55\text{ GHz}} \simeq 0.8$
 271 is roughly consistent with the X-ray spectral index of the lobe measured by *Suzaku*. The lobe
 272 is approximated as a sphere with the radius $R_\ell = 185\text{ kpc}$, so that the emission region volume is
 273 $V_\ell = (4/3)\pi R_\ell^3$.

274 For the lobe, we use a similar model as for the outer jet region discussed above, but include in
 275 addition extragalactic background light (EBL) photons within the infrared-to-optical range as tar-
 276 get photon field for the inverse-Compton scattering (‘EC/(CMB+EBL)’ model). In the calculations
 277 we use the EBL model of Mazin & Raue (2007) and account for Klein-Nishina effects. The choice
 278 of a particular EBL parameterization does not affect the model results because of the negligible
 279 contribution of the EC/EBL emission component to the γ -ray emission of the lobe within the LAT
 280 energy range. We neglect the contribution of the host galaxy to the target photon field because of
 281 the large distance of the analyzed NW lobe from the center ($15' \simeq 450\text{ kpc}$). Finally, we assume
 282 homogeneous distributions of the radiating electrons and of the magnetic field within the lobe.

283 In the framework of the applied simplified model, the γ -ray flux of 2FGL J1629.4+8236 can
 284 be accounted for reasonably well (see Figure 4, thick gray line) by the inverse-Compton emission
 285 of the lobe for the following parameters: the equipartition ratio $\eta_{\text{eq}} \equiv U_e/U_B = 45$, magnetic field
 286 intensity $B = 0.37\ \mu\text{G}$, and the electron energy distribution of a double-broken power-law form
 287 $n_e(\gamma) \propto \gamma^{-s_1}$ for $\gamma_{\text{min}} \leq \gamma \leq \gamma_{\text{br}}$ and $n_e(\gamma) \propto \gamma^{-s_2} \exp[-\gamma/\gamma_{\text{max}}]$ for $\gamma > \gamma_{\text{br}}$ with $s_1 = 2.0$,
 288 $s_2 = 2.5$, $\gamma_{\text{min}} = 1$, $\gamma_{\text{br}} = 3 \times 10^3$, and $\gamma_{\text{max}} = 10^6$. With the above model parameters, the lobe
 289 pressure stored in ultrarelativistic electrons and magnetic field is $p_{\text{e+B}} \simeq 8.4 \times 10^{-14}\text{ dyn cm}^{-2}$.
 290 The total energy of the structure, being a sum of the work done in displacing a volume V_ℓ of
 291 surrounding gas at pressure $p_{\text{e+B}}$, namely $p_{\text{e+B}} V_\ell$, and the energy of the material inside the cavity,
 292 $p_{\text{e+B}} V_\ell / (\hat{\gamma} - 1)$ (assuming ultrarelativistic equation of state with the adiabatic index $\hat{\gamma} = 4/3$), is
 293 then $E_{\text{tot}} \simeq 4 p_{\text{e+B}} V_\ell \sim 3 \times 10^{59}\text{ erg}$. The lobe’s lifetime can be estimated as $t_\ell \sim E_{\text{tot}}/L_j \sim$
 294 $10 \times (L_j/10^{45}\text{ erg s}^{-1})\text{ Myr}$. We note that any significant proton contribution to the lobe pressure
 295 would increase the evaluated values of E_{tot} and t_ℓ .

296 The EC/(CMB+EBL) model fits the data quite well, and the emerging lobe’s parameters seem
 297 reasonable. The implied departure from the energy equipartition is rather large, $\eta_{\text{eq}} = 45$, but still
 298 within the range 1 – 100 established for the lobes in radio galaxies with X-ray measurements alone
 299 (e.g. Kataoka & Stawarz 2005; Croston et al. 2005; Isobe et al. 2011). Furthermore, the expected
 300 cooling timescale for the electrons emitting the observed $\gtrsim 1\text{ GeV}$ photons, i.e., electrons with
 301 energies $\gamma \lesssim \gamma_{\text{max}} = 10^6$, is roughly $t_{\text{cool}} \simeq 2.1 \times (\gamma/10^6)^{-1}\text{ Myr}$. Meanwhile, assuming a typical
 302 drift velocity of electrons in the lobe (or expansion velocity of the lobe) $v_{\text{lobe}} \lesssim 0.1\ c$, one can infer
 303 that these γ -ray emitting electrons can travel only $d \simeq 65 \times (v_{\text{lobe}}/0.1\ c) \times (\gamma/10^6)^{-1}\text{ kpc}$ before
 304 they cool radiatively. This scale is much smaller than the extension of the NW lobe in NGC 6251

305 (~ 0.5 Mpc). Interestingly, this finding resembles the case of the giant lobes in Centaurus A, and
 306 similarly suggests efficient in-situ re-acceleration of the radiating particles within the whole vol-
 307 ume of the giant lobe (see the discussion in Abdo et al. 2010d). Moreover, in both the Centaurus A
 308 and NGC 6251 radio galaxies, the γ -ray detections imply that the lobes emit one to two orders of
 309 magnitude more energy in γ -rays than at radio/sub-mm wavelengths.

310 Finally we note that the non-thermal pressure of the NW lobe in NGC 6251, $\sim 10^{-13}$ dyn cm $^{-2}$,
 311 seems comparable with/bit less than the thermal pressure of the surrounding gaseous medium,
 312 $p_{\text{th}} \sim (10^{-13} - 10^{-12})$ dyn cm $^{-2}$ at the distances $200'' - 1000''$ from the core. The thermal pressure
 313 was estimated by Evans et al. (2005) based on the extrapolation of the X-ray halo profile associated
 314 with the group of galaxies including NGC 6251 and detected by *Chandra* and XMM-*Newton* (see
 315 also in this context Birkinshaw & Worrall 1993; Sambruna et al. 2004a). Such an extrapolation
 316 may not provide a realistic estimate however, and should rather be considered as an upper limit
 317 for the ambient medium pressure. This, together with a likely contribution of (mildly) relativis-
 318 tic protons to the lobe’s internal pressure, may suggest that either the extended radio structures
 319 in NGC 6251 are in a pressure equilibrium with the environment, or that these are over-pressured
 320 cavities, so that the expansion of the giant lobes in the system is still pressure-driven on Mpc scale
 321 (basically beyond the extension of the thermal halo of the surrounding group of galaxies).

322 5. Conclusions

323 We have presented a *Suzaku* X-ray observation of the NW lobe in a nearby radio galaxy
 324 NGC 6251. Through this observation, we found for the first time non-thermal diffuse X-ray emis-
 325 sion associated with the NW lobe. Since the error circle of the γ -ray source 2FGL J1629.4+8236
 326 contains *both* the NW lobe and outer jet region, we discussed the possible origin of γ -ray emission
 327 by detailed modeling of the spectral energy distributions assuming a synchrotron plus inverse-
 328 Compton emission on CMB background photons. We argued that, at least at energies below 10
 329 GeV, the observed γ -ray emission is well explained by non-thermal emission from the NW lobe
 330 rather than from the outer jet region, with reasonable physical parameters (such as magnetic field,
 331 electron density etc) expected in radio lobes in general. Since the spatial extent of the NGC 6251
 332 radio lobe is quite large (~ 0.5 Mpc), and the expected radiative cooling time is much shorter
 333 for γ -ray emitting electrons, efficient in-situ acceleration of radiative particles is necessary within
 334 the whole volume of the giant lobe. We also briefly discussed the non-thermal pressure stored
 335 in ultrarelativistic electrons and magnetic field (not considering a likely contribution of relativistic
 336 proton) of the NW lobe in NGC 6251, which is estimated as $\sim 10^{-13}$ dyn cm $^{-2}$ from the model, and
 337 it seems comparable with or somewhat less than the thermal pressure of the surrounding gaseous
 338 medium.

339 L.S. is grateful for the support from Polish MNiSW through the grant N-N203-380336. C.C.C.'s
340 work at NRL was supported by NASA DPR S-15633-Y.

REFERENCES

- 341
- 342 Abdo, A. A., Ackermann, M., Ajello, M., et al. 2010a, *ApJS*, 188, 405
- 343 Abdo, A. A., Ackermann, M., Ajello, M., et al. 2010b, *ApJ*, 715, 429
- 344 Abdo, A. A., Ackermann, M., Ajello, M., et al. 2010c, *ApJ*, 720, 912
- 345 Abdo, A. A., Ackermann, M., Ajello, M., et al. 2010d, *Science*, 328, 725
- 346 Abdo, A. A., et al. 2011, *ApJS*, in press (arXiv:1108.1435)
- 347 The Pierre Auger Collaboration: Abraham, J., Abreu, P., et al. 2007, *Science*, 318, 938
- 348 Ackermann, M., Ajello, M., Allafort, A., et al. 2011a, *ApJ*, 743, 171
- 349 Ackermann, M., Ajello, M., Allafort, A., et al. 2011b, *ApJ*, in press (arXiv:1109.4678)
- 350 Birkinshaw, M., & Worrall, D. M. 1993, *ApJ*, 412, 568
- 351 Celotti, A., Ghisellini, G., & Chiaberge, M. 2001, *MNRAS*, 321, L1
- 352 Cheung, C. C. 2007, *The First GLAST Symposium*, 921, 325
- 353 Croston, J. H., Hardcastle, M. J., Harris, D. E., et al. 2005, *ApJ*, 626, 733
- 354 Day, C., et al., 1998, *The ASCA Data Reduction Guide*, Tech. Rep., (Greenbelt: NASA GSFC),
355 v.2.0
- 356 Dickey, J. M., & Lockman, F. J. 1990, *ARA&A*, 28, 215
- 357 Evans, D. A., Hardcastle, M. J., Croston, J. H., Worrall, D. M., & Birkinshaw, M. 2005, *MNRAS*,
358 359, 363
- 359 Evans, D. A., Summers, A. C., Hardcastle, M. J., et al. 2011, *ApJ*, 741, L4
- 360 Ferrarese, L., & Ford, H. C. 1999, *ApJ*, 515, 583
- 361 Georganopoulos, M., Sambruna, R. M., Kazanas, D., et al. 2008, *ApJ*, 686, L5
- 362 Hardcastle, M. J., Harris, D. E., Worrall, D. M., Birkinshaw, M., et al. 2004, *ApJ*, 612, 729

- ³⁶³ Hardcastle, M. J., Cheung, C. C., Feain, I. J., & Stawarz, Ł. 2009, *MNRAS*, 393, 1041
- ³⁶⁴ Ho, L. C. 2002, *ApJ*, 564, 120
- ³⁶⁵ Ishisaki, Y., Maeda, Y., Fujimoto, R., et al. 2007, *PASJ*, 59, 113
- ³⁶⁶ Isobe, N., Seta, H., Gandhi, P., & Tashiro, M. S. 2011, *ApJ*, 727, 82
- ³⁶⁷ Kataoka, J., & Stawarz, Ł. 2005, *ApJ*, 622, 797
- ³⁶⁸ Kokubun, M., Makishima, K., Takahashi, T., et al. 2007, *PASJ*, 59, 53
- ³⁶⁹ Koyama, K., Tsunemi, H., Dotani, T., et al. 2007, *PASJ*, 59, 23
- ³⁷⁰ Laing, R. A., Riley, J. M., & Longair, M. S. 1983, *MNRAS*, 204, 151
- ³⁷¹ Mack, K.-H., Klein, U., O’Dea, C. P., & Willis, A. G. 1997a, *A&AS*, 123, 423
- ³⁷² Mack, K.-H., Kerp, J., & Klein, U. 1997b, *A&A*, 324, 870
- ³⁷³ Mazin, D., & Raue, M. 2007, *A&A*, 471, 439
- ³⁷⁴ Matsushita, K., Ohashi, T., & Makishima, K., 2000, *PASJ*, 52, 685
- ³⁷⁵ Migliori, G., Grandi, P., Torresi, E., et al. 2011, *A&A*, 533, A72
- ³⁷⁶ Mitsuda, K., Bautz, M., Inoue, H., et al. 2007, *PASJ*, 59, 1
- ³⁷⁷ Moskalenko, I. V., Stawarz, Ł., Porter, T. A., & Cheung, C. C. 2009, *ApJ*, 693, 1261
- ³⁷⁸ Mukherjee, R., Halpern, J., Mirabal, N., & Gotthelf, E. V. 2002, *ApJ*, 574, 693
- ³⁷⁹ O’Sullivan, S., Reville, B., & Taylor, A. M. 2009, *MNRAS*, 400, 248
- ³⁸⁰ Pe’er, A., & Loeb, A. 2011, arXiv:1111.3964
- ³⁸¹ Perley, R. A., Bridle, A. H., & Willis, A. G. 1984, *ApJS*, 54, 291
- ³⁸² Rees, N. 1990, *MNRAS*, 244, 233
- ³⁸³ Sambruna, R. M., Gliozzi, M., Donato, D., et al. 2004a, *A&A*, 414, 885
- ³⁸⁴ Sambruna, R. M., Gambill, J. K., Maraschi, L., et al. 2004b, *ApJ*, 608, 698
- ³⁸⁵ Schoenmakers, A. P., de Bruyn, A. G., Röttgering, H. J. A., & van der Laan, H. 2001, *A&A*, 374,
³⁸⁶ 861

- ³⁸⁷ Serlemitsos, P. J., Soong, Y., Chan, K.-W., et al. 2007, PASJ, 59, 9
- ³⁸⁸ Stawarz, Ł., Sikora, M., Ostrowski, M., & Begelman, M. C. 2004, ApJ, 608, 95
- ³⁸⁹ Stawarz, Ł., Siemiginowska, A., Ostrowski, M., & Sikora, M. 2005, ApJ, 626, 120
- ³⁹⁰ Takahashi, T., Abe, K., Endo, M., et al. 2007, PASJ, 59, 35
- ³⁹¹ Tawa, N., Hayashida, K., Nagai, M., et al. 2008, PASJ, 60, 11
- ³⁹² Tavecchio, F., Maraschi, L., Sambruna, R. M., & Urry, C. M. 2000, ApJ, 544, L23
- ³⁹³ Waggett, P. C., Warner, P. J., & Baldwin, J. E. 1977, MNRAS, 181, 465
- ³⁹⁴ Wegner, G., Bernardi, M., Willmer, C. N. A., et al. 2003, AJ, 126, 2268
- ³⁹⁵ Willott, C. J., Rawlings, S., Blundell, K. M., & Lacy, M. 1999, MNRAS, 309, 1017
- ³⁹⁶ Voges, W., Aschenbach, B., Boller, T., et al. 1999, A&A, 349, 389

Table 1: *Suzaku* XIS observation log.

Target Name	R.A. [deg]	Dec. [deg]	Exposure [ks]	Obs. Start Time (UT)
NGC6251_LOBE	246.5880	82.6370	34.2	2011 Apr 15 06:37:27
NGC6251_LOBE_BGD1	247.8200	82.9170	18.8	2011 Apr 16 00:38:47
NGC6251_LOBE_BGD2	245.4460	82.3530	12.1	2011 Apr 16 10:25:32

Table 2: Fitting parameters for the power-law model.

Parameter	Value
N_{H} [cm^{-2}]	5.54×10^{20} (fixed)
Γ	1.90 ± 0.15
$K_{1\text{keV}}$ [$\text{keV}^{-1} \text{cm}^{-2} \text{s}^{-1}$]	$(9.11 \pm 0.91) \times 10^{-5}$
$\chi^2/\text{d.o.f}$	20.54/14
$P(\chi^2)$	1.14×10^{-1}
$F_{0.4-7.5\text{keV}}$ [$\text{erg cm}^{-2} \text{s}^{-1}$]	4.07×10^{-13}
$L_{0.4-7.5\text{keV}}$ [erg s^{-1}]	5.4×10^{41}

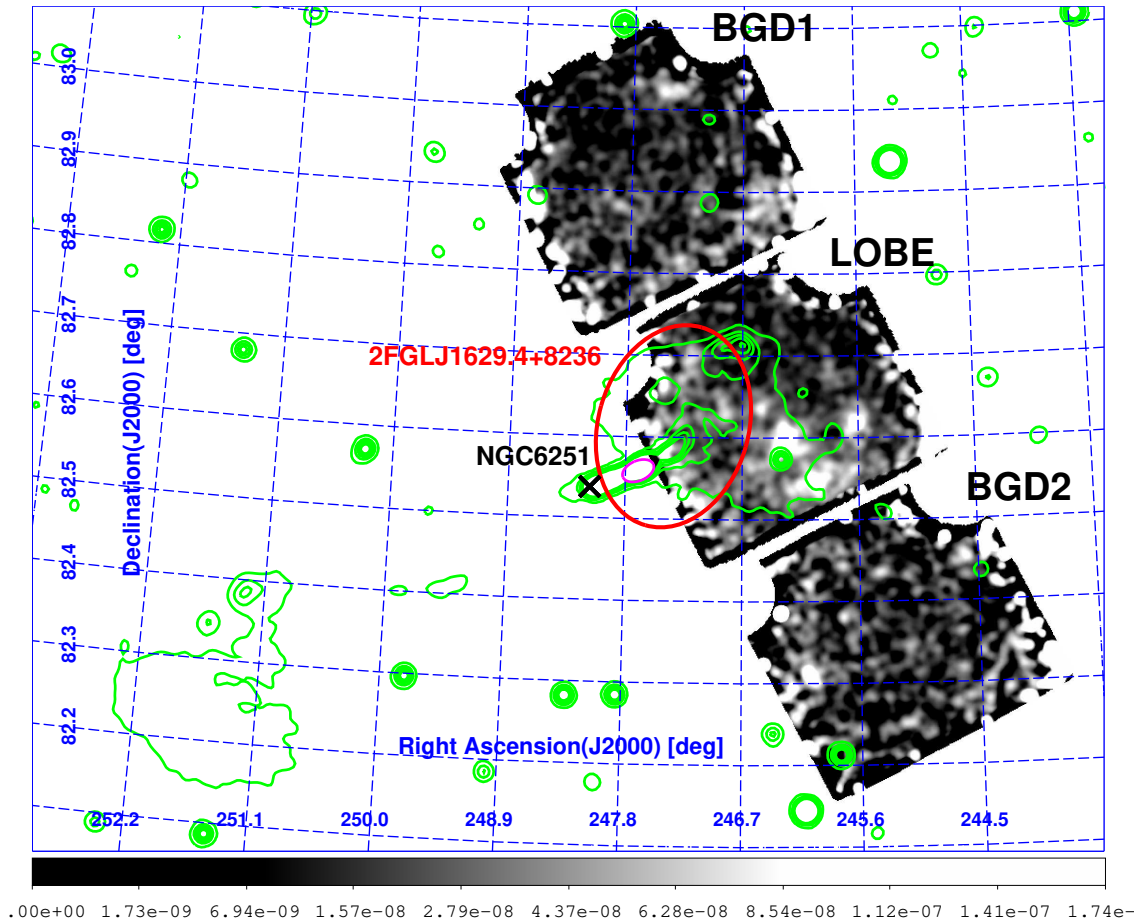


Fig. 1.— *Suzaku* X-ray image of the NW lobe in NGC 6251 (vignetting and exposure corrections applied). Data from XIS 0 and XIS 3 are summed in the 0.4 – 10 keV energy band. The image shows the relative excess of smoothed photon counts (arbitrary units indicated in the bottom bar) and displayed with square root scaling. The green contours denote the large-scale radio structure of the source observed by *WSRT* at 55'' resolution (Mack et al. 1997a) and indicate levels of 8, 31, 54, 77 and 100 mJy/beam. The red ellipse denotes the 95% position error of 2FGL J1629.4+8236. The position of the radio core of NGC 6251 is marked by the black cross at the center and the adjacent ‘outer jet region’ is marked by the magenta ellipse.

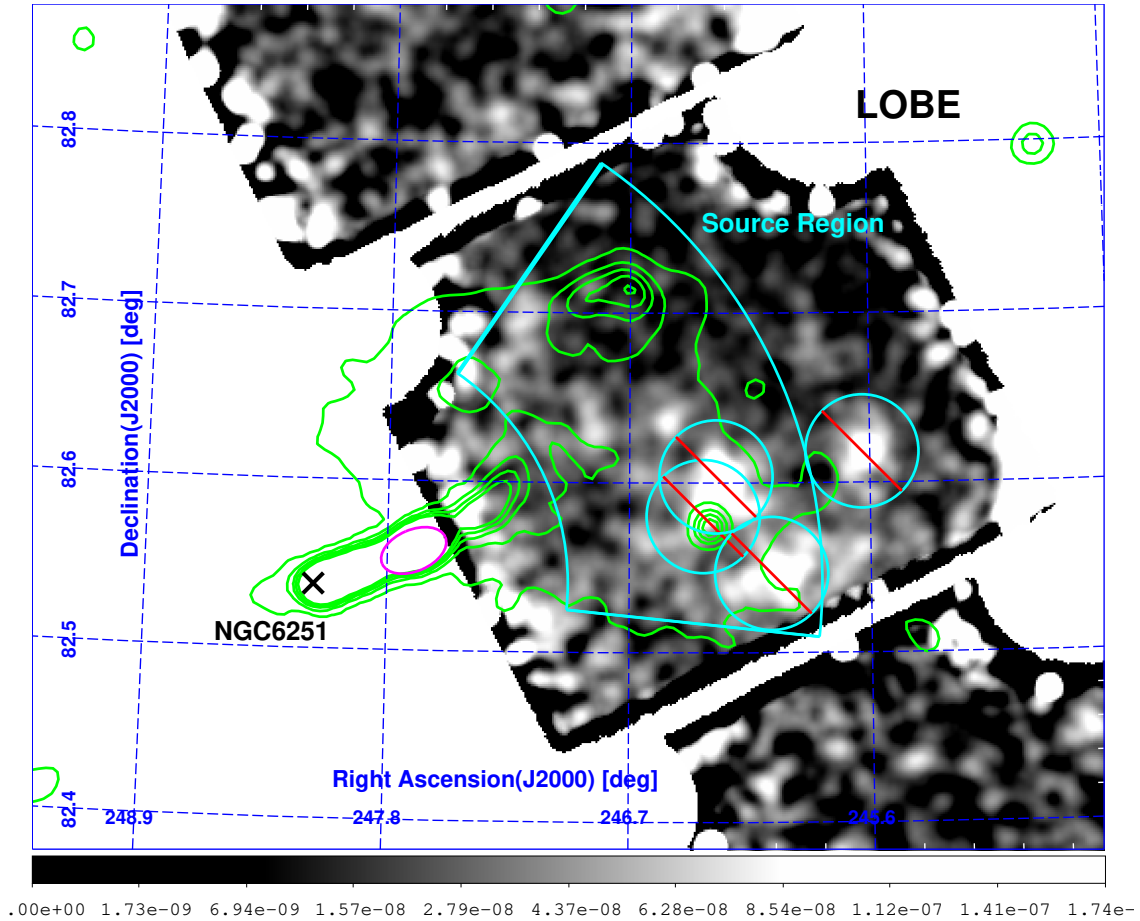


Fig. 2.— Same as Figure 1, but zooming into the NW lobe region. The *Suzaku* source extraction region is denoted by the cyan contours. The point X-ray sources removed from the analysis are marked by cyan circles with red stripes.

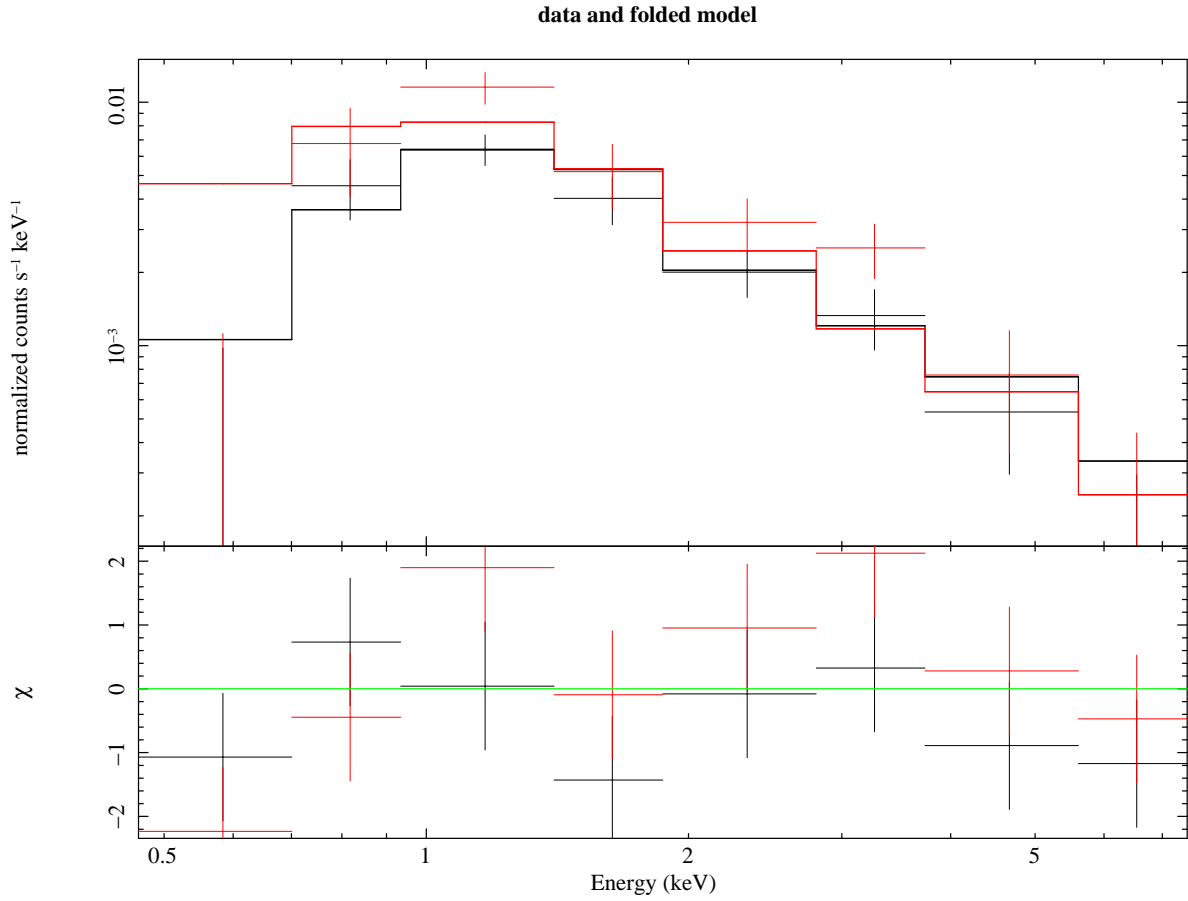


Fig. 3.— *Suzaku* XIS spectra of the diffuse emission component coinciding with the NW lobe of NGC 6251 in the photon energy range 0.4 – 7.5 keV, fitted by the model $wabs \times power-law$. The XIS0 + XIS3 and XIS1 spectra are shown in black and red, respectively.

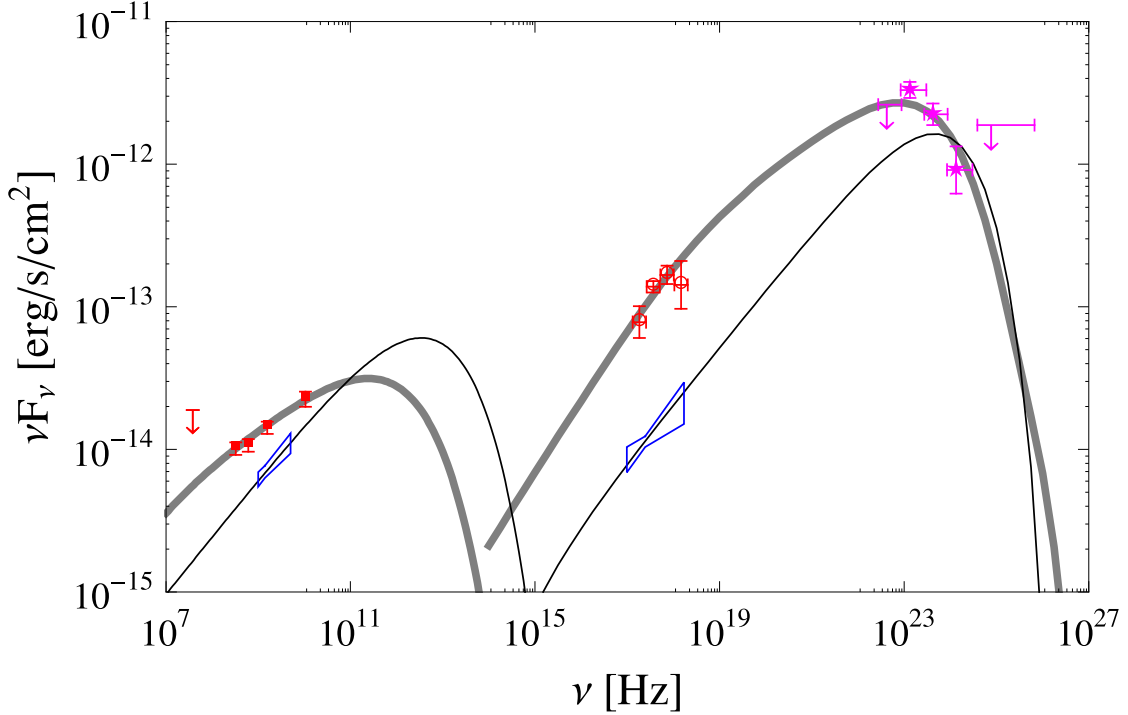


Fig. 4.— Broad-band spectral energy distributions of the outer jet and the NW lobe in NGC 6251, including the *Fermi*-LAT source 2FGL J1629.4+8326. The radio and X-ray data for the outer jet (blue bow-ties) are from (Sambruna et al. 2004a, based on the maps presented in Perley et al. 1984), and Evans et al. (2005), respectively (see § 4.1). The radio fluxes of the NW lobe (red squares and red arrow) are described in section 4.2. The X-ray fluxes for the lobe, as found in this paper, are given in the 0.5 – 1.0 keV, 1.0 – 2.0 keV, 2.0 – 4.0 keV, and 4.0 – 8.0 keV bins (open red circles). Finally, the LAT fluxes of 2FGL J1629.4+8326 (magenta stars) are taken from the 2FGL catalog (Abdo et al. 2011). Thin solid line represents the beamed IC/CMB model for the outer jet (see § 4.1), assuming the association with 2FGL J1629.4+8326. Thick gray line represent the IC/(CMB+EBL) model for the NW lobe (see § 4.2), again assuming the association with 2FGL J1629.4+8326.